Simulation of fractional-order low-pass filters

Thomas Hélie

***Abstract*—The attentuation of standard analog low-pass filters corresponds to a multiple value of -6 decibels per octave. This quantified value is related to the order of the filter. The issue addressed here is concerned with the extension of integer orders to non integer orders, such that the attenuation of a low-pass filter can be continuously adjusted. Fractional differential systems are known to provide such asymptotic behaviors and many results about their simulation are available. But even for a fixed cutoff frequency, their combination does not generate an additive group with respect to the order and they involve stability problems. In this paper, a class of low-pass filters with orders between 0 (the filter is a unit gain) and 1 (standard one-pole filter) is defined to restore these properties. These infinite dimensional filters are not fractional differential but admit some well-posed representations into weighted integrals of standard one-pole filters. Based on this, finite dimensional approximations are proposed and recast into the framework of state-space representations. A special care is given to reduce the computational complexity, through the dimension of the state. In practice, this objective is reached for the complete family, without damaging the perceptive quality, with dimension 13. Then, an accurate low-cost digital version of this family is built in the time-domain. The accuracy of the digital filters is verified on the complete range of parameters (cutoff frequencies and fractional orders). Moreover, the stability is guaranteed, even for time-varying parameters. As an application, a plugin has been implemented which provides a new audio tool for tuning the cutoff frequency and the asymptotic slope in a continuous way. As a very special application, choosing a one-half order combined with a low cutoff frequency (20Hz or less), the filter fed with a white noise provides a pink noise generator.**

***Index Terms*—Irrational transfer function, Fractional order, Simulation, State-space methods, Signal synthesis.**

Note: A few sound examples are available at
`http://recherche.ircam.fr/anasyn/helie/TASLP-FractionalFilter`

I. INTRODUCTION

Low-pass filters are widely used in electronic music. For standard analog circuits, their attenuation corresponds to a multiple value of -6 decibels per octave, beyond some cutoff frequency. This quantified value is related to the order of the filter. Thus, typical configurations that are used in analog synthetizers are -6 decibels per octave for a one-pole filter (order 1), -12 decibels per octave (order 2), and -24 decibels per octave (order 4). But, there is no standard configuration for which intermediate values can be found, such as -3 decibels per octave, which would correspond to a one half order.

In this paper, we consider a family of causal stable filters with fractional order $0 \leq \alpha \leq 1$. In the frequency domain, their attenuation corresponds to -6α decibels per octave. Thus, cascading such a filter with any standard filter (of integer order) allows the synthesis of any attenuation slope beyond the cutoff frequency. The main difficulty to cope with such filters is that they do not correspond to any finite dimensional differential system and that their transfer functions are not rational. Hence, finite dimensional approximations and efficient digital versions must be derived for the complete family.

Some first results have been established in [1], from which the perceptive relevance of the family of filters had been tested and confirmed. However, these results had three practical limitations. First, filters with integer and non-integer orders had to be processed separately so that a (simple but) special interpolation had to be derived when order $\alpha \in (0,1)$ approached the boundary values 0 and 1. Second, to be accurate enough, the approximated filters had to be of dimension larger than about 20. Third, because of the numerical scheme used in [1], the phase of the digital filters was a bit poor in the high frequency range.

The results proposed in this paper remove the first limitation while significantly improving the two other ones. In particular, the approximation with dimension 13 proposed here appear to be sufficient and even better than the previous solution (with dimension 20). Moreover, the complete family of the approximated digital filters is proved to be stable, including for time-varying parameters. This has also been practically checked using a real-time version (implemented in FAUST language). As a special case, these results can be straightforwardly used to produce a low-compution real-time generator of *pink noise*. Indeed, for $\alpha = 1/2$ and using a low cutoff frequency (such as 20 Hz or less), the digital filter behaves in the audio range as a fractional integrator of order one half (slope of -3 decibels per octave over the all audio frequency range). When this filter is excited by white noise, this is known to produce a *pink noise*, as detailed in [2].

This paper is organized as follows. Section II defines the family of filters. Section III gives some of their properties. It introduces well-posed representations of the associated infinite dimensional systems. They correspond to continuous aggregations of one-pole filters (also so-called "diffusive representation"). In section IV, finite dimensional approximations are derived. Two methods of approximation are examined. The first one is based on a finite dimensional interpolation of the original infinite state. The second one is based on an optimization with respect to an audio measure. This second method fits better with the objective. In section V, these approximations are used to derive a finite dimensional state-space representation of the complete family, in the continuous-time domain. A diagonal form is obtained. Then, digital versions of the family of filters are proposed in section VI, with a special

Thomas Hélie is with IRCAM - CNRS UMR 9912 - UPMC, 1, place Igor Stravinsky, 75004 Paris, France e-mail: thomas.helie@ircam.fr

care to both the low computational complexity and stability issues, including for time-varying parameters. Section VII presents simulations and results which are compared with the original exact family. Finally, section VIII gives a short discussion about the second method in relation with other standard techniques.

II. FAMILY OF FILTERS

A. Motivation

A causal stable first-order low-pass filter with cutoff frequency f_c and with unit gain is described by the transfer function $H_1\big(s/(2\pi f_c)\big)$ where $H_1(s) = 1/(s+1)$ is defined in the complex Laplace half-plane

$$\mathbb{C}_0^+ = \big\{s \in \mathbb{C} \big| \Re e(s) > 0\big\}.$$

The corresponding impulse response is $h_1(2\pi f_c t)$ with $h_1(t) = \exp(-t)$ for positive times and 0 otherwise. The cascade of $n \geq 2$ of these filters yields the same results with $H_n(s) = H_1(s)^n$, $h_n(t) = \big(t^{n-1}/(n-1)!\big)\exp(-t)$. More generally, introducing $H_0(s) = 1$ and $h_0 = \delta$ (Dirac measure), the following property is straightforward: if p and q are non negative integers, $H_p\, H_q = H_{p+q}$ and $h_p \star h_q = h_{p+q}$ (additive group of filters with respect to the order).
This paper aims at extending this family of filters and this property to any non negative real order $r \in \mathbb{R}_+$. The difficulty is concerned with the fractional part $0 \leq \alpha < 1$ of the order $r = [r] + \alpha$ ($[r] \in \mathbb{N}$), to which the following of the paper is devoted.

B. Definition

We consider the family of stable causal low-pass filters, described by the transfer functions defined in the complex Laplace half-plane $\mathbb{C}_0^+$ by

$$F_{\alpha,f_c}(s) = H_\alpha\Big(\frac{s}{2\pi f_c}\Big) \quad (1)$$

$$\text{with } H_\alpha(s) = \frac{1}{(s+1)^\alpha}, \quad (2)$$

where function $P_\alpha : z \mapsto z^\alpha$ ($\alpha > 0$) is the analytic continuation of the positive root for positive z over the complex plane $\mathbb{C}$ except on the branch cut $\mathbb{R}^-$. Note that in F_{α,f_c}, the complex variable $s = \sigma + i\omega$ is a scale unit variable where $-\sigma$ stands for a damping (in s^{-1}) and ω is an angular frequency (in $\mathrm{rd.s}^{-1}$). In H_α, the same labels correspond to normalized dimensionless variables. For sake of conciseness, these variables will be used according to the same convention in the following, without ambiguity.

The impulse response is positive and is given by [3, (29.3.11)]

$$f_{\alpha,f_c}(t) = h_\alpha(2\pi f_c t) \quad (3)$$

$$\text{with } h_\alpha(t) = \frac{t^{\alpha-1}}{\Gamma(\alpha)}\mathrm{e}^{-t} \text{ if } t > 0 \text{ and 0 otherwise,} \quad (4)$$

where $\Gamma(\alpha) = \int_0^{+\infty} t^{\alpha-1}\mathrm{e}^{-t}\,\mathrm{d}t$ denotes the factorial function. For non integer orders α, such an impulse response corresponds to an infinite dimensional system, as detailed in section III.

In this paper, parameter α is real and greater than 0 (filter is identity) and lower than 1 (standard one pole filter). Inside this range, the impulse response (4) is singular at $t = 0$ and has a non standard decreasing behavior. Parameter f_c is typically a frequency inside the audio range ($F^- = 20$ Hz to $F^+ = 20$ kHz). It corresponds to the tuning frequency of the filter: this is the standard -3dB cutoff frequency if $\alpha = 1$ and corresponds to a -3α dB cutoff frequency in the general case. On the Fourier axis, the asymptotic behavior of $f \mapsto F_{\alpha,f_c}(2i\pi f) = 1/(1 + if/f_c)^\alpha$ corresponds to:

(i) a unit gain if $f \ll f_c$;
(ii) a "-6α dB/octave" behavior with phase $-\alpha \times 90$ degrees if $f \gg f_c$.

Bode diagrams are displayed in figure 1.

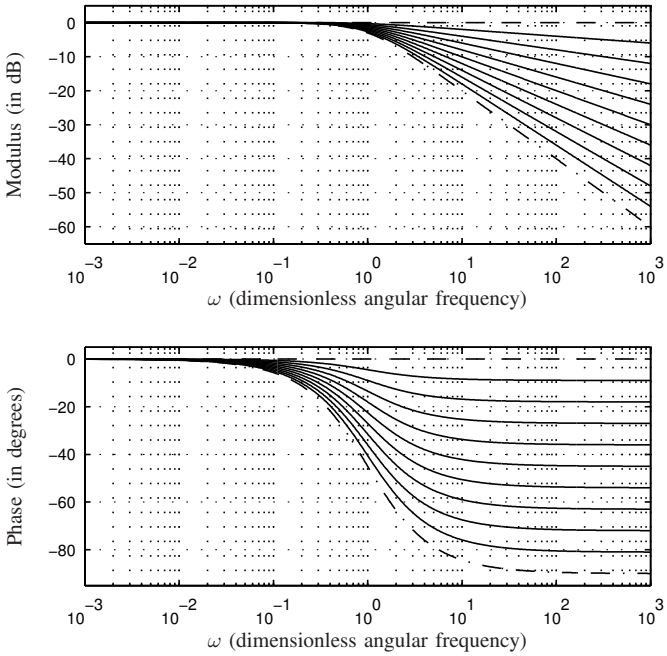

Fig. 1. Bode diagrams of H_α ($s = i\omega$), where ω is the dimensionless angular frequency, for fractional orders α increasing from 0 (curve at the top, - -) to 1 (curve at the bottom ---) with step 0.1. Bode diagrams of F_{α,f_c} are the same, replacing $\omega = 1$ by the frequency f_c (in Hz).

C. Remarks

Such filters can be encountered in physics and especially in some materials produced in electrical engineering. Examples are the admittances of coils, or some copper wires formed into a serpentine structure, or some electric materials involving "skin effects" [4]. More generally, this filter is known to model the so-called Cole-Davidson dielectric relaxation [5], [6].

Note that another family of filters with similar asymptotic behaviors (i-ii) corresponds to the fractional differential systems defined by $G_\alpha(s) = 1/(s^\alpha + 1)$. There is a large amount of work about these systems, as witnessed by e.g. [7], [8], [9], [10] and references therein. However, the family G_α is not investigated here because, contrarily to H_α, it has a number of weaknesses for audio applications. First, it does not provide a natural extension of the "filter order" with respect to the cascade. Second, the stability is not fulfilled on the wide range

$\alpha > 0$ [11]. Third, some impulse responses involve regular oscillations ($g_2(t) = \sin(t)$ for positive times) whereas the behavior of the family is wanted to be "regular" and without resonance, as for the reference first-order filter.

III. INFINITE DIMENSIONAL REPRESENTATION

The family of filters defined by (1-4) does not correspond to any standard ARMA filter. Moreover, it is ill-suited to be approximated by short finite impulse responses: there is a singularity at $t = 0$ and the decay is not fast enough. However, it benefits from some properties and exact representations that can be exploited as a first step, in order derive efficient ARMA approximations. More precisely, in the Laplace domain, the singularities are not reduced to poles as usual, but define a continuous set, namely, a "cut" (or "branch cut"). This section details this first step and properly introduce this information, which is precisely the one that is used in the sequel to build "efficiently informed" approximations.

A. Properties

For $0 < \alpha < 1$, transfer function H_α is irrational so that it does not correspond to any finite order filter. However, several standard properties are fulfilled.

Indeed, H_α is hermitian symmetric ($\overline{H_\alpha(\overline{s})} = H_\alpha(s)$), analytic and bounded on $\mathbb{C}_0^+$ with norm $\|H_\alpha\|_{\mathbb{H}^\infty} = 1$ for the Hardy space $\mathbb{H}^\infty(\mathbb{C}_0^+)$ (see appendix IX-A for some recalls on the definition and basic properties). This implies that it corresponds to a causal stable system with finite gain (of maximal value $\|H_\alpha\|_{\mathbb{H}^\infty} = 1$) which maps a real input to a real output.

More precisely, because of its asymptotic low-pass behavior, H_α also belongs to the Hardy spaces $\mathbb{H}^\beta(\mathbb{C}_0^+) \supset \mathbb{H}^\infty(\mathbb{C}_0^+)$ for all $\beta > 1/\alpha$. This implies that for $\alpha > 1/2$, the impulse response of the system has a finite energy. This is not the case otherwise.

Moreover, according to the definition of $P_\alpha : z \mapsto z^\alpha$ used in (2), H_α admits a (hermitian symmetric) analytic continuation over $\mathbb{C} \setminus \mathcal{C}$ with branch cut $\mathcal{C} = -1 + \mathbb{R}^-$, where $\setminus$ denotes the set difference. This cut is the locus of the singularities of the transfer function H_α (for $0 < \alpha < 1$) in the Laplace domain. It corresponds to the half-line starting from the branch point $s = -1$ (the pole of H_1) and going to $s = -\infty$.

B. Integral formalism

Following [12], an exact representation of H_α is given by an integral of one-pole filters, with respect to an appropriate measure M, where the poles σ describe the cut $\mathcal{C}$. It is given by, for all $s \in \mathbb{C}_0^+$,

$$\begin{aligned} H_\alpha(s) &= \int_{\mathcal{C}} \frac{M_\alpha(\mathrm{d}\sigma)}{s-\sigma}, \\ \text{with } M_\alpha(\mathrm{d}\sigma) &= \mu_\alpha(\sigma)\,\mathrm{d}\sigma, \end{aligned} \tag{5}$$

where, for all $\sigma \in \mathcal{C}$, the density $\mu_\alpha(\sigma) = \big(H_\alpha(\sigma - i\,0^+) - H_\alpha(\sigma + i\,0^+)\big)/(2i\pi)$ corresponds in this case to the positive function

$$\mu_\alpha(-1-\xi) = \frac{\sin(\alpha\pi)}{\pi\xi^\alpha}, \text{ for } \xi > 0. \tag{6}$$

Note that in (5), μ_α plays the same role for the continuous sum over the cut $\mathcal{C}$ as the residues for a discrete sum over a countable set of poles. More precisely, as the measure $M_\alpha(\mathrm{d}\sigma)$ is absolutely continuous with respect to the Lebesgue measure, the density can be derived by applying the residues theorem for an adapted (oriented) Bromwich contour (see appendix IX-B for some recalls). An integral representation such as (5) (sometimes denominated *diffusive representation* if the cut is a subset of $\mathbb{R}^-$) is well-posed provided that M_α fulfills the criterion (see e.g. [13, § 5-6] and [14])

$$\int_{\mathcal{C}} \left| \frac{\mathrm{d}M_\alpha(\sigma)}{1-\sigma} \right| < +\infty.$$

This is the case here.

From (5-6), the transfer function H_α is given by, for all $s \in \mathbb{C}_0^+$,

$$H_\alpha(s) = \int_{\mathcal{C}} \frac{\mu_\alpha(\sigma)}{s-\sigma}\mathrm{d}\sigma = \int_0^{+\infty} \frac{\sin(\alpha\pi)}{\pi\xi^\alpha}\,\frac{1}{s-(1+\xi)}\,\mathrm{d}\xi. \tag{7}$$

The impulse response corresponding to (7) is

$$h_\alpha(t) = \int_{\mathcal{C}} e_\sigma^+(t)\; M_\alpha(\mathrm{d}\sigma) = \int_0^{+\infty} \frac{\sin(\alpha\pi)}{\pi\xi^\alpha}\, e_{-1-\xi}^+(t)\,\mathrm{d}\xi, \tag{8}$$

where $e_\sigma^+(t) = \mathrm{e}^{\sigma t}\,1_{\mathbb{R}_+}(t)$ is the causal exponential associated with the one-pole filter $E_\sigma : s \mapsto \frac{1}{s-\sigma}$.

Moreover, the filter with impulse response (8) can be realized (in the sense of the system theory), using the following infinite set of first order differential systems, for all $t \in \mathbb{R}^+$ and $\sigma \in \mathcal{C}$,

$$\partial_t x(\sigma,t) = \sigma\, x(\sigma,t) + u(t), \text{ with } x(\sigma,0) = 0, \tag{9}$$

$$y(t) = \int_{\mathcal{C}} x(\sigma,t)\, M_\alpha(\mathrm{d}\sigma)\,, \tag{10}$$

that is, a state-space representation with input $u(t)$, infinite dimensional state $x(\cdot,t)$ and output $y(t)$.

Finally, following (1), a well-posed diffusive representation of $F_{\alpha,\eta}$ is obtained by replacing s in (5) by its scaled version $s/(2\pi f_c)$. Accordingly, t must be replaced by $2\pi f_c t$ in (8), and ∂_t by $\frac{1}{2\pi f_c}\,\partial_t$ in (9).

IV. FINITE DIMENSIONAL APPROXIMATIONS

In order to obtain simulations, finite dimensional approximations of diffusive representations (5-10) are built, based on a finite set of poles σ_n localized on the cut $\mathcal{C}$, that is,

$$\widehat{H}_\alpha(s) = \sum_{n=1}^{N} \frac{\mu_n(\alpha)}{s-\sigma_n}. \tag{11}$$

The issue addressed below is concerned with the poles placement and the estimation of weights μ_n. Two methods, detailed in [12], are tested with parameters which are specially designed for the family of filters described in (1-2).

A. Accuracy requirements

To get accurate approximations of F_{α,f_c} on the audible range ($F^-=20\,\text{Hz}$ to $F^+=20\,\text{kHz}$) for any cutoff frequency f_c in the same range, function $\omega \mapsto H_\alpha(s=i\omega)$ must be accurately approximated on

(i) the (dimensionless) angular frequency range $\omega_{min}=\frac{F^-}{F_c^+}=10^{-3}$ to $\omega_{max}=\frac{F^+}{F_c^-}=10^{+3}$.

Additionally, we consider the other following features based on simplified principles of audio perception [15]:

(ii) frequencies are perceived according to a logarithmic scale;

(iii) gain deviations are perceived relatively to the reference gains.

B. Method 1: interpolation of the state

As proposed in [16] and [12, § 4.1], a first method consists of approximating the state $x(\sigma,t)$ ($\sigma\in\mathcal{C}$) over a bounded part of the cut by an interpolation derived from a finite subset of states ($x(\sigma_n,t)$ for $1\le n\le N$).

According to (ii), the poles σ_n's are chosen as

$$\sigma_n=-1-\xi_n=-1-10^{\ell_n}\in\mathcal{C},\ \text{for}\ 0\le n\le N+1, \qquad (12)$$

where the ℓ_n's are equally spaced, with step $\delta=\frac{\ell_{N+1}-\ell_0}{N+1}$, from ℓ_0 to ℓ_{N+1} (see [12, example 2]) for typical values for a fractional integrator of order $1/2$).

Then, the output y in (10) is built from the (exact) state variables $x_n(t)=x(\sigma_n,t)$ $(1\le n\le N)$ by considering the interpolated state $\widehat{x}(\sigma,t)$ in place of $x(\sigma,t)$, where

$$\widehat{x}(\sigma,t)=\sum_{n=1}^{N}\Lambda\Big(\frac{L(\sigma)-\ell_n}{\delta}\Big)\,x_n(t), \qquad (13)$$

with the standard "hat interpolation" function $\Lambda(\eta)=\big(1-|\eta|\big)\,1_{[-1,1]}(\eta)$, and for the log-scale variable $\ell=L(\sigma)=\log_{10}(-\sigma-1)$, corresponding to (12).

For this approximation, equation (10) yields $\widehat{y}(t)=\sum_{n=1}^{N}\mu_n(\alpha)x_n(t)$ with

$$\begin{aligned}\mu_n(\alpha) &= \int_{\mathcal{C}}\Lambda\Big(\frac{L(\sigma)-\ell_n}{\delta}\Big)M_\alpha(\mathrm{d}\sigma)\\ &= \frac{\sin(\alpha\pi)}{\pi}\,\frac{\kappa\big((1-\alpha)\delta\ln 10\big)}{1-\alpha}\,\xi_n^{1-\alpha}, \qquad (14)\end{aligned}$$

where $\kappa(w)=2\big(\cosh(w)-1\big)/w$ is such that $\kappa(w)\sim w$ if $0\le w\ll 1$. Note that compared to [12], the log-scale adaptation in the interpolation (through L_n) allows the exact computation of the μ_n's. Finally, equations (11) with (12) and (14) define a family of ARMA filters of order N, with closed-form expressions with respect to α, namely, with $\xi_n=10^{\ell_n}$,

$$\widehat{H}_\alpha(s)=\frac{\sin(\alpha\pi)}{\pi}\,\frac{\kappa\big((1-\alpha)\delta\ln 10\big)}{1-\alpha}\sum_{n=1}^{N}\frac{\xi_n^{1-\alpha}}{s+1+\xi_n}.$$

In practice, an appropriate range for the poles corresponds to $\ell_0=-10$ and $\ell_{N+1}=+10$. Results are displayed for $N=20$ poles in figure 2, and $N=40$ poles in figure 3. Their observation shows that they are usable for $N=20$ and accurate for $N=40$. In practice, the trend observed on the regularity

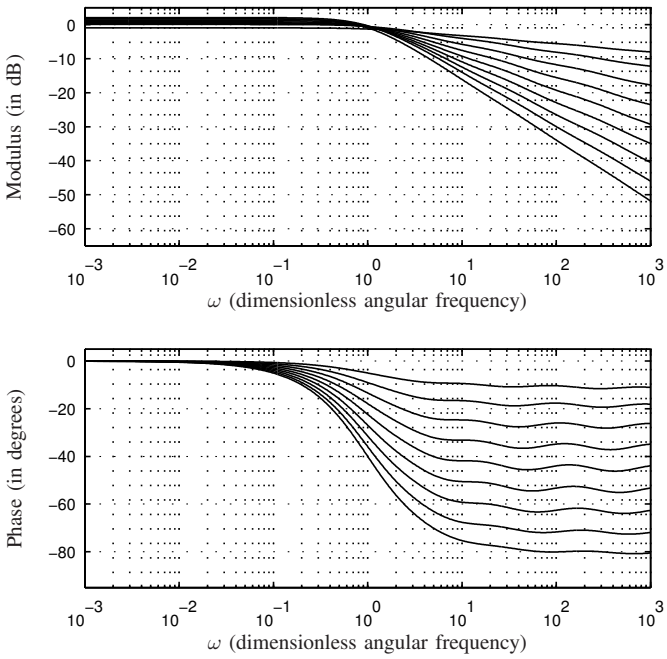

Fig. 2. (Interpolation, $N=20$) Bode diagrams of $\widehat{H}_\alpha$ ($s=i\omega$) for fractional orders α increasing from 0.1 (top) to 0.9 (bottom) with step 0.1 for $\ell_0=-10$, $\ell_{N+1}=+10$. These curves are to be compared with those of figure 1.

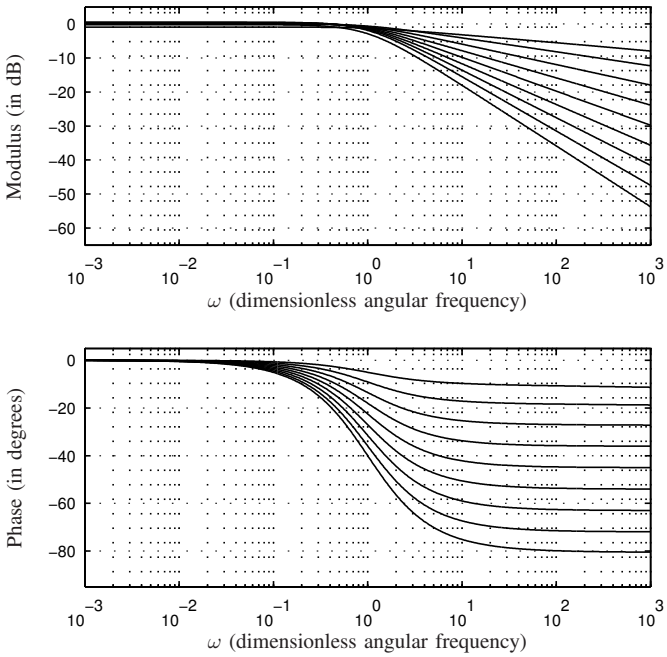

Fig. 3. (Interpolation, $N=40$) Idem as in figure 2 for $N=40$.

of the shapes between $N = 20$ and $N = 40$ continue when increasing the number of poles N. In this sense, this method provides a set of results with an increasing quality: they appear to be qualitatively acceptable for audio applications and they allows the selection of a complexity according to one target CPU load. However, from the mathematical point of view, it suffers from severe drawbacks: first, the maximal error over the (useful dimensionless) range $\omega \in [10^{-3}, 10^{+3}]$ saturates for orders $\alpha \neq 0.5$ meaning that even if the shape seems to be better when increasing the order, biases appear; second, even for $\alpha = 0.5$, the convergence towards 0 is quite slow. These numerical observations supported by the figure 4 clearly allow for opportunities for further mathematical investigations.

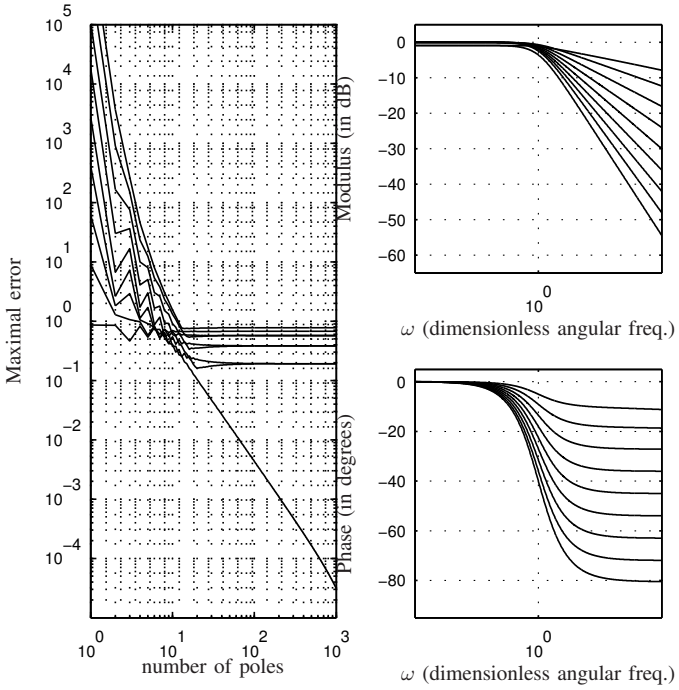

Fig. 4. (Interpolation, $1 \leq N \leq 1000$ for fractional orders α increasing from 0.1 to 0.9 with step 0.1 for $\ell_0 = -10$, $\ell_{N+1} = +10$) Left: the maximal error $E_{max} = \max_{\omega \in [10^{-3}, 10^3]} \left| H_\alpha(i\omega) - \widehat{H}_\alpha(i\omega) \right|$ decreases for $\alpha = 0.5$ and saturates for other orders; Right: Bode diagrams of $\widehat{H}_\alpha$ $(s = i\omega)$ for $N = 1000$.

But, for practical reasons about real time issues, the following section focuses on *reducing the dimension N while preserving (or even increasing) the accuracy*, rather than improving the asymptotic behaviour of the method 1: a second method is used below, for which the μ_n's are optimized.

C. Method 2: optimization of weights

Rewrite the finite dimensional model (11) as

$$\widehat{H}_\alpha(s) = \boldsymbol{E}_{\boldsymbol{\sigma}}(s)^T \boldsymbol{\mu}(\alpha), \qquad (15)$$

$$\text{with } \boldsymbol{E}_{\boldsymbol{\sigma}}(s) = \begin{pmatrix} \frac{1}{s-\sigma_1} \\ \vdots \\ \frac{1}{s-\sigma_N} \end{pmatrix} \text{ and } \boldsymbol{\mu} = \begin{pmatrix} \mu_1 \\ \vdots \\ \mu_N \end{pmatrix},$$

where the weights $\boldsymbol{\mu}$ are real-valued in order to preserve the hermitian symmetry of the transfer function. To optimize the weights $\boldsymbol{\mu}$, we consider the objective function proposed in [12], defined from (15) by

$$G(\boldsymbol{\mu}) = \int_{\omega_{min}}^{\omega_{max}} \left| 1 - \frac{\widehat{H}_\alpha(s = i\omega)}{H_\alpha(s = i\omega)} \right|^2 \mathrm{d} \ln \omega, \qquad (16)$$

which takes the audio features (i-iii) into account.

In practice, a discretized version of G must be considered to allow numerical computations: the integral in (16) is approximated by a finite sum on an appropriate frequency grid, here, $\ln \omega_k = \ln \omega_{min} + \frac{k}{K} \ln \frac{\omega_{max}}{\omega_{min}}$ for $0 \leq k \leq K$. Moreover, a regularization term is required to avoid ill-conditioned matrix inversion if $N = \dim(\boldsymbol{\mu})$ is not sufficiently small. We use a standard Tikhonov penalty term [17], [18] which is proportional to $\boldsymbol{\mu}^T \boldsymbol{\mu}$.

This yields the following practical objective function

$$\begin{aligned} \widehat{G}(\boldsymbol{\mu}) &= \sum_{k=1}^{K} \left| 1 - \frac{\widehat{H}_\alpha(s = i\omega_{k-\frac{1}{2}})}{H_\alpha(s = i\omega_{k-\frac{1}{2}})} \right|^2 (\ln \omega_k - \ln \omega_{k-1}) \\ &\quad + \varepsilon \boldsymbol{\mu}^T \boldsymbol{\mu} \\ &= \overline{(\boldsymbol{M}\boldsymbol{\mu} - \boldsymbol{H})}^T \boldsymbol{W} (\boldsymbol{M}\boldsymbol{\mu} - \boldsymbol{H}) + \varepsilon \boldsymbol{\mu}^T \boldsymbol{\mu}, \end{aligned} \qquad (17)$$

where, for $1 \leq k \leq K$, $\omega_{k-\frac{1}{2}} = \sqrt{\omega_{k-1}\omega_k}$ denotes the geometric mean of ω_{k-1} and ω_k, matrix $\boldsymbol{M}$ is composed of the rows $[\boldsymbol{M}]_{k,*} = \boldsymbol{E}_{\boldsymbol{\sigma}}(s = i\omega_{k-\frac{1}{2}})^T$ defined in (15), vector $\boldsymbol{H}$ is composed of $[\boldsymbol{H}]_k = H_\alpha(s = i\omega_{k-\frac{1}{2}})$, the diagonal matrix $\boldsymbol{W}$ is defined by $[\boldsymbol{W}]_{k,k} = (\ln \omega_k - \ln \omega_{k-1}) \,/\, \left| [\boldsymbol{H}]_k \right|^2$.

The minimization of (17) is straightforward: first, the complex values in $\boldsymbol{M}$ and $\boldsymbol{H}$ are decomposed into their real and imaginary parts ($z = x + iy$), so that the objective function is re-expressed as a real nonnegative function of exclusively real quantities with respect to the real-valued vector μ_n; second, this standard least square problem is analytically solved; third, the analytic result is recomposed into a closed form with respect to the complex quantities for conciseness. This yields the real-valued optimal weights

$$\boldsymbol{\mu}^{opt} = \left[\overline{\boldsymbol{M}}^T \boldsymbol{W} \boldsymbol{M} + \varepsilon I_N \right]^{-1} \mathcal{R}e\left(\overline{\boldsymbol{M}}^T \boldsymbol{W} \boldsymbol{H} \right). \qquad (18)$$

If the condition number of the inverse matrix is larger than the targeted precision (here, that of *floats*), no regularization is needed so that the Tikhonov penalty parameter is set to $\varepsilon = 0$. Otherwise, there is no general rule to select this parameter [19], [20]. Here, we use a basic iterative dichotomy: (step $n = 0$) we introduce $\varepsilon_0^- = 0$ (bad condition number) and a value $\varepsilon_0^+ > 0$ sufficiently large to provide a condition number that is better than the target; (step n+1) if $\varepsilon_n^* = (\varepsilon_n^- + \varepsilon_n^+)/2$ provides a condition number that is better than the target, we set $\varepsilon_{n+1}^- = \varepsilon_n^-$, $\varepsilon_{n+1}^+ = \varepsilon_n^*$, and otherwise, we set $\varepsilon_{n+1}^- = \varepsilon_n^*$, $\varepsilon_{n+1}^+ = \varepsilon_n^+$; the sequence is stopped when the targeted condition number obtained for ε_n^* is reached (with a margin of factor 2).

Compared to § IV-B, some adaptations of parameters appear to be relevant in practice. In order to reject ripples near the boundaries of the useful range $[10^{-3}, 10^3]$, the range $[\omega_{min}, \omega_{max}]$ used in the objective function is enlarged to $[10^{-4}, 10^4]$. Moreover, when significantly reducing the number

N poles, it appears that contracting the range of the poles is also relevant, corresponding to $\ell_0 = -5$ and $\ell_{N+1} = +5$.

Here, results are displayed for $N = 20$ in figure 5, and $N = 10$ in figure 6.

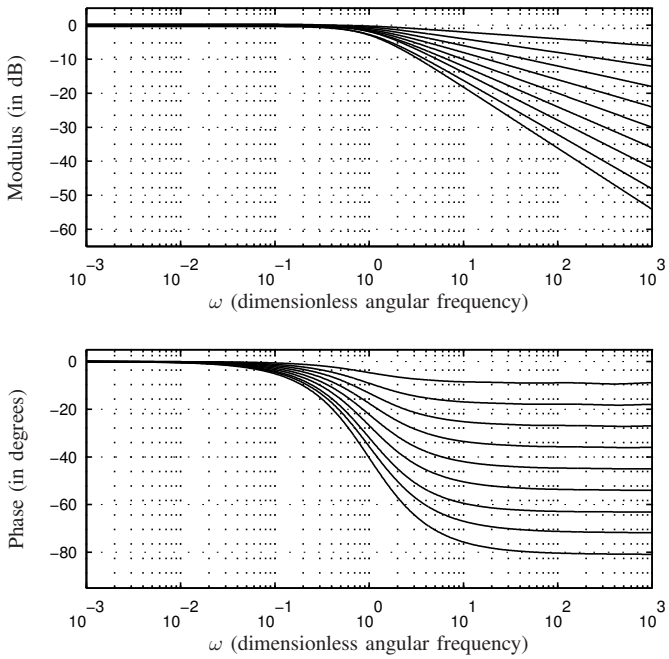

Fig. 5. (Optimization, $N = 20$) Bode diagrams of $\widehat{H}_\alpha$ ($s = i\omega$) for fractional orders α increasing from 0.1 (top) to 0.9 (bottom) with step 0.1. Parameters are $\ell_0 = -5$, $\ell_{N+1} = +5$, $\omega_{min} = 10^{-4}$, $\omega_{max} = 10^{+4}]$ and $\varepsilon \sim 10^{-13}$. These curves are to be compared with those of figure 2.

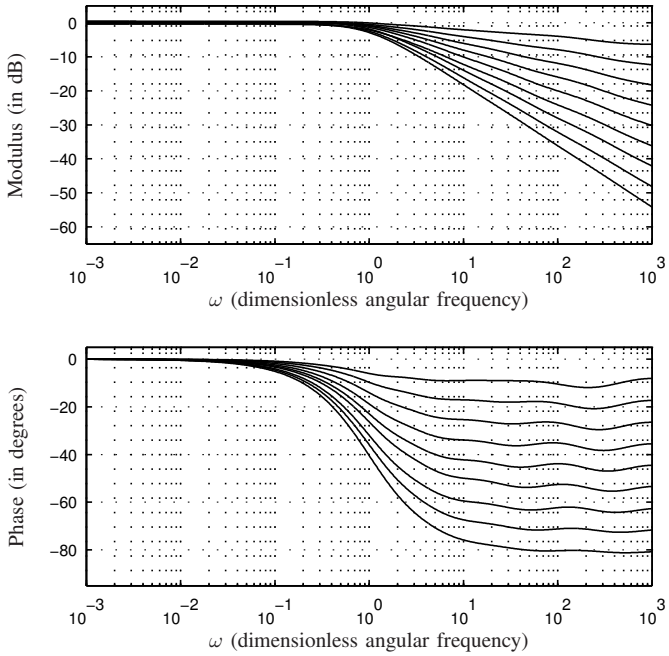

Fig. 6. (Optimization, $N = 10$) Idem as in figure 5 for $N = 10$, with $\varepsilon \sim 5 \times 10^{-14}$.

D. Observation and first conclusion

In practice, approximations based on optimizations appear to be better than those based on interpolations: in figures 2 to 6, similar qualities are obtained with twice fewer poles for optimization than for interpolation.

An interpretation is that the method based on interpolations fully depends on the approximation quality of each analytic density μ_α through a refined mesh whereas that based on optimization is less contraining. Indeed, this last method only exploits the structural information which is shared by the family of (infinite dimensional) filters, namely, the cut. In this sense, it acutely combines a structural information which is not obvious to identify by most of blind methods, with the flexibility and the efficiency of such "blind" approximation methods, according to "scalings, dimensions and measures" of audio interest.

At this step, parameters $\ell_0 = -5$, $\ell_{N+1} = +5$, $\omega_{min} = 10^{-4}$, $\omega_{max} = 10^{+4}$ for $N = 20$ poles and a regularization about $\varepsilon \sim 10^{-13}$ yield a good trade-off. This will still be improved by optimizing the parameters of the global representation of the family which is introduced below.

V. STATE-SPACE REPRESENTATION

A. Representation of the complete family up to the limit oders

Consider a (fixed) vector of N poles $\boldsymbol{\sigma}$ defined as in section IV. A finite dimensional state-space representation, with input $u \in \mathbb{R}$, state $x \in \mathbb{R}^{N+1}$ and output $y \in \mathbb{R}$, which approximates the complete family of filters F_{α,f_c} ($f_c > 0$ and $0 \leq \alpha \leq 1$) is given by

$$\frac{1}{2\pi f_c}\partial_t x = A\,x + B\,u, \tag{19}$$

$$y = C(\alpha)\,x + D(\alpha)\,u, \tag{20}$$

where $A = \mathrm{diag}(-1;\sigma)$ is a constant diagonal matrix of dimension $(N+1) \times (N+1)$, $B = [1,\ldots,1]^T$ is a constant vector ($(N+1) \times 1$), and where matrix C ($1 \times (N+1)$) and D (1×1) exclusively depend on α, as detailed below.

In order to handle the limit orders $\alpha = 0$ and $\alpha = 1$, we introduce the equally-spaced sequence $\alpha_j = j/J$ for $0 \leq j \leq J$, and where J is a fixed mesh number which is chosen to linearly interpolate orders α_j. Indeed, for $\alpha = \alpha_0 = 0$, the filter is a unit gain so that $C = C_0 = [0,\ldots,0]$ and $D = D_0 = 1$. For $\alpha = \alpha_J = 1$, the filter is a one-pole filter and $C = C_J = [1,0,\ldots,0]$ and $D = D_J = 0$. For $\alpha = \alpha_j$ with $1 \leq j \leq J-1$, an approximation of the filter is obtained for $C = C_j = [0, \boldsymbol{\mu}(\alpha_j)^T]$ and $D_j = 0$ where $\boldsymbol{\mu}(\alpha_j)$ is computed as in section IV, using methods 1 or 2 for $\alpha = \alpha_j$. For other values, the filter is approximated using a linear interpolation of C_j and D_j as follows:
if $\alpha_j \leq \alpha \leq \alpha_{j+1}$ (with $0 \leq j \leq J-1$), then

$$C(\alpha) = (j+1-J\alpha)C_j + (J\alpha - j)C_{j+1} \tag{21}$$

$$D(\alpha) = (j+1-J\alpha)D_j + (J\alpha - j)D_{j+1}. \tag{22}$$

This allows fast calculations of functions $C(\alpha)$ and $D(\alpha)$ from a set of (J+1) pre-computed matrices C_j and D_j. Moreover, the approximation introduced by (21-22) can be reduced as much as desired by increasing J. For instance, for

$J = 60$, the maximal gain deviation $20\log_{10}\left|H_{\alpha_j}/H_{\alpha_{j+1}}\right|$ is lower than 1 dB (which is only reached at $f = 20\,kHz$ for $f_c = 20\,Hz$).

Aside from giving a continous interpolation of the filters over the complete range $0 \leq \alpha \leq 1$, without considering special treatments for the limit orders, equations (19-22) can also be used to advantage in order to improve the quality of the approximation, as detailed below.

B. Optimized approximation used for the simulation

The direct gain D and the pole $2\pi f_c[A]_{1,1}$ have been included in (19-20) to tackle the limit cases $\alpha = 0$ and $\alpha = 1$, respectively. As they introduce some additional computations, an interesting issue is to take them into account in the optimization method (method 2): equation (15) has simply to be modified by including functions $s \mapsto 1$ and $s \mapsto 1/(s+1)$ in $\boldsymbol{E}_{\boldsymbol{\sigma}}(s)$ and including the associated weights (D and $[C]_1$) in $\boldsymbol{\mu}$.

In practice, this significantly improves the results, especially below the cutoff frequency, while equations (19-22) are not modified.

Thus, considering $N + 1 = 13$ poles with $\ell_0 = -1$ and $\ell_N = 5$ leads to accurate approximations for the complete family. Moreover, for these parameters, no Tikhonov penalty is required in the objective function ($\varepsilon = 0$). These results are displayed in figure 7. The detailed contributions of all the individual one-pole filters (including the constant gain filter $D(\alpha)$) are displayed in figure 8. This figure shows that:

- for the poles with a high index, the perceptible information is concentrated in the phase in the high frequency range;
- since the objective function (16) involves a log-frequency measure ($\mathrm{d}\ln\omega$) as in the Bode diagram, the law which is naturally adapted to the poles placement is $-\xi_n$ with $\xi_n = 10^{\eta_n}$ from $\eta_0 = 0$ to $\eta_N = \ln\omega_{max}$; the grid chosen in (12) (concatenated with $\xi = -1$ and rearranged) is similar to this law with a slightly refined mesh near the cutoff angular frequency $\omega = 1$, so that it improves the approximations in this critical frequency area.

This last result is chosen to build the simulation proposed below. The approximation error (maximal with respect to the dimensionless range $\omega \in [10^{-3}, 10^{3}]$) is displayed versus the number of poles (N+1) and several orders α in figure 9. This error provides a bound which is available for all the cutoff frequencies over all the audible frequency range. For N+1=13 poles, this relative error is less than 1.5×10^{-3} (2.47×10^{-3} and 1.13×10^{-3} for 12 and 14 poles respectively). Over 14 poles, the gain in accuracy becomes much smaller.

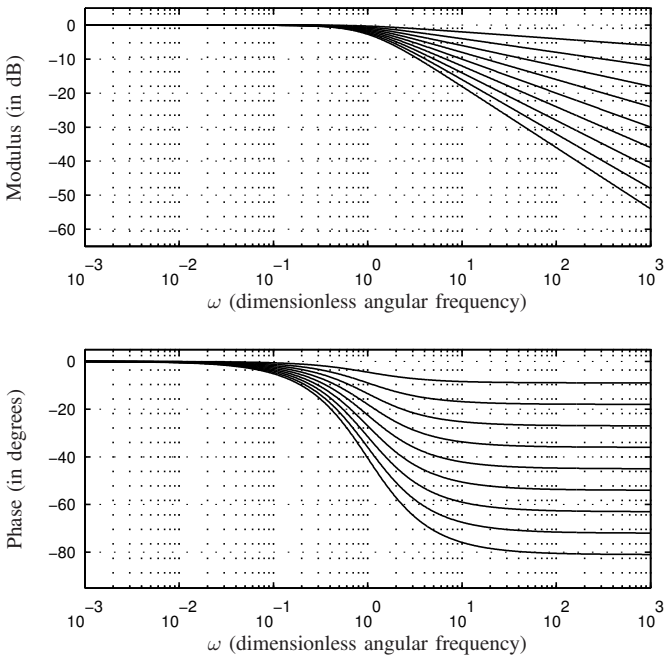

Fig. 7. Bode diagram obtained for the state-space representation (19-22) of dimension $N + 1 = 13$, optimized for paremeters $\varepsilon = 0$, $\ell_0 = -1$ and $\ell_N = +5$.

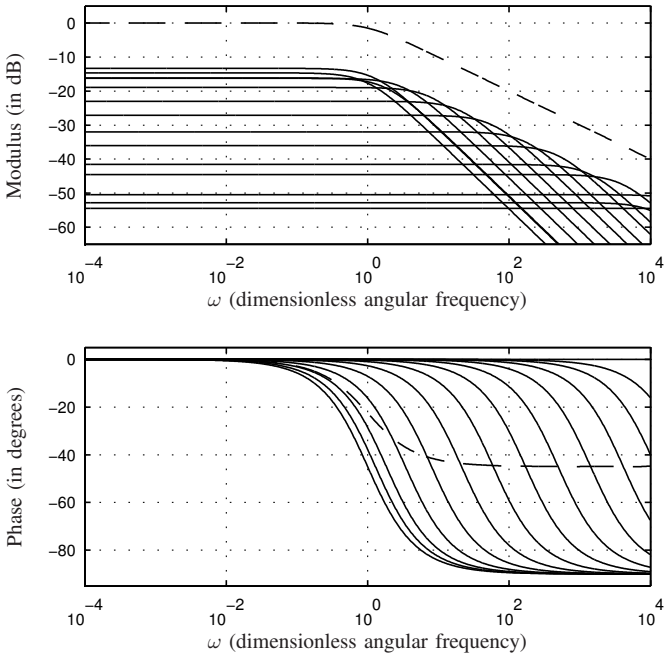

Fig. 8. Bode diagrams of the approximated filter for $\alpha = 0.5$ in dashed line and of the individual one-pole filters (including the constant gain filter $D(\alpha)$) in solid lines. The optimization is performed on the range $\omega \in [10^{-4}, 10^{+4}]$ which includes the usefull range $\omega \in [10^{-3}, 10^{+3}]$.

VI. DISCRETE TIME DOMAIN

This section is concerned with the discrete-time simulation of the differential system (19), that is, the computation of $X(m) = x(mT_s)$ from $U(m) = u(mT_s)$ ($m \in \mathbb{N}$), for the sampling frequency $f_s = 1/T_s$.

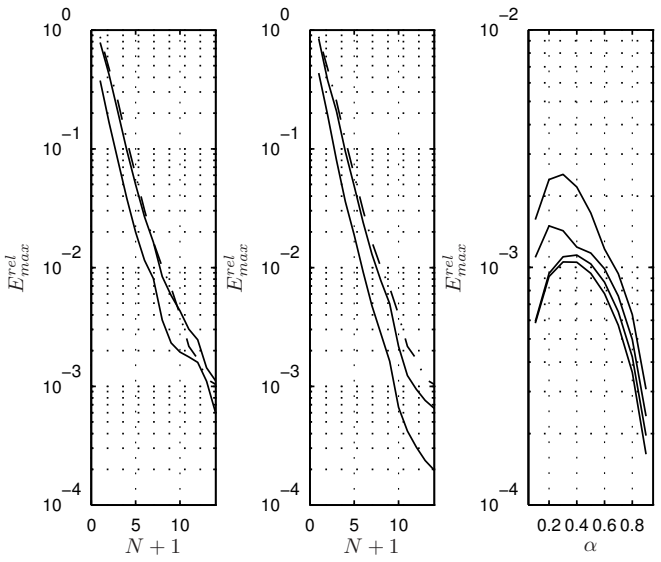

Fig. 9. Maximal relative error $E_{max} = \max_{\omega\in[10^{-3},10^{3}]} \left|1 - \frac{\widehat{H}_\alpha(i\omega)}{H_\alpha(i\omega)}\right|$: (left) error versus the number of poles $N+1$ for fractional orders α increasing from 0.1 (-) to 0.5 (- -) with step 0.2; (center) idem from 0.5 (- -) to 0.9 (-); (right) error versus α for N+1=12, 13, 14 and 15 poles. The error increases from $\alpha = 0$ (error is zero) to a maximal value between 0.2 and 0.5 (depending on the number of poles) and decreases to zero at $\alpha = 1$.

A. Choice of a numerical scheme

Numerous numerical methods are available for simulating ordinary differential equations (see e.g. [21]) and finite-dimensional state-space systems (see e.g. [22]). Basic ones are the Euler (forward or backward, respectively) methods: their main disavantage is that they strongly distort the pole mapping $s \mapsto z = \exp(s\,T)$ which is exact if $|\Im m(s)| < \pi f_s/2$, and that they do not preserve the stability domain (under or over stabilization, respectively). For these reasons, these methods are discarded here.

A second family of methods is based on expontential integrators, which provide an ideal pole mapping (so, the stability domain) and restore exact free regimes. The approximation is introduced on the input through the choice of its interpolation (from samples). Typical interpolations are sample-and-hold or affine interpolations. A third method often used for audio applications is based on the bilinear transform (also called the "Tustin's method"): a transfer function G in the Laplace domain is approximated by $G_d(z) = G\big(S(z)\big)$ in the z-domain, using the mapping $S(z) = \frac{2}{T}\frac{1-z^{-1}}{1+z^{-1}}$. Although the pole mapping is not exact, the bilinear transformation exactly preserves the stability domain and avoids the problem of aliasing because it maps the Fourier axis ($s = i\omega \in i\mathbb{R}$) and the left-half complex plane $\mathbb{C}_0^+$ onto the unit circle and the unit disk in the z-plane, respectively.

These two last family of methods have been applied to the state-space representation described in section V-B for an over-sampling ratio 2. Bode diagrams computed from impulse response have been compared, for several parameters α and f_c. It appears that the modulus is more accurate for exponential integrators (especially for the sample-and-hold approximation) than for the bilinear transform. But, it is the opposite for the phase.

Alternative modified versions of Tustin's method based on interpolations between Tustin's method and the backward Euler methods have been designed in order to improve the magnitude frequency response of digital integrators and differentiators. One first mapping corresponds to the nonminimum phase integrator $1/S(z) = \frac{T}{2}\frac{1+\gamma+(1-\gamma)z^{-1}}{1-z^{-1}}$, and a second one is the associated minimum phase integrator. These mappings are usually tuned choosing $\gamma = 3/4$ in order to restore an accurate magnitude at the half Nyquist frequency (see [23] for a more detailed presentation). For this reason, they have even been used for the design of digital fractional differentiators and integrators [24]. However, contrarily to Tustin's method, these modified versions do not map the Fourier axis onto the unit circle: the original phase constancy (with respect to the positive/negative frequencies) is significantly damaged, which makes the approximation error on $s \mapsto 1+s$ and H_α increase, even with the over-sampling ratio 2.

For all these reasons, the bilinear transform is chosen in the following. In practice, this choice provides an acceptable trade-off on the modulus and the phase with the over-sampling factor. Moreover, it only requires standard floating point operations and avoids the computation of the exponential for the pole mapping.

B. Discrete state-space representation

Equation (19) rewrites

$$\partial_t x = A_c\, x + B_c\, u, \tag{23}$$

with $A_c(f_c) = 2\pi f_c\, A$ and $B_c(f_c) = 2\pi f_c\, B$.

Combined with (20), this state-space representation approximates F_{α,f_c} defined in (1-2) by

$$\widehat{F}_{\alpha,f_c}(s) = C(\alpha)\big(s\,I - A_c(f_c)\big)^{-1} B_c(f_c) + D(\alpha), \tag{24}$$

in the Laplace domain. A discrete state-space representation

$$X(m+1) = A_d\, X(m) + B_d\, U(m), \tag{25}$$
$$Y(m) = C_d\, X(m) + D_d\, U(m), \tag{26}$$

which restores the bilinear transform, that is, which is such that $C_d\big(I - z^{-1}\,A_d\big)^{-1} B_d + D_d = \widehat{F}_{\alpha,f_c}\Big(\frac{2}{T}\frac{1-z^{-1}}{1+z^{-1}}\Big)$, is derived using the Cayley transform (see e.g. [25]). Introducing $\nu = 2/T$ and $Q = \big(\nu I - A_c\big)^{-1}$, matrices are given by

$$\begin{aligned} A_d &= \big(\nu I + A_c\big)\, Q, \\ B_d &= \sqrt{2\nu}\, Q\, B_c, \\ C_d &= \sqrt{2\nu}\, C\, Q, \\ D_d &= \widehat{F}_{\alpha,f_c}(\nu) = C\, Q\, B_c + D. \end{aligned}$$

C. Low-complexity digital fractional-order filter

As A_d is diagonal, equation (25) describes a set of decoupled first order AR filters. This involves 2N+2 products and N+1 sums. The observation equation (26) involves N+2 products and N+1 sums. The total amounts are then 3N+3 products and 2N+2 sums.

The amount of products can be reduced to only 2N+2 products, by using a change of state $X = \mathrm{diag}(B_d)Z$ so that B_d become a vector of unit gains. This leads to

$$Z_n(m+1) = -a_n^c\, Z_n(m) + U(m), \quad \text{for } 1 \le n \le N+1 \tag{27}$$
$$Y(m) = G^c(\alpha)\, Z_n(m) + D^c(\alpha)\, U(m), \tag{28}$$

where $a_n^c = [-A_d]_{n,n}$, $G^c = C_d\,\mathrm{diag}(B_d)$, $D^c = D_d$.

In the z domain, this corresponds to the transfer function

$$\widetilde{F}_{\alpha,f_c}(z) = \sum_{n=1}^{N+1} \frac{G_n^c(\alpha)}{1 + a_n^c z^{-1}} + D^c(\alpha).$$

Coefficients depending on f_c are marked with a superscript c, those depending on α are written as functions of α. Introducing $q_n^c = 1/(1-\omega_n^c)$, they are given by

$$a_n^c = -(1+\omega_n^c)q_n^c, \tag{29}$$
$$G_n^c(\alpha) = 2\omega_c\,(q_n^c)^2\, C_n(\alpha), \tag{30}$$
$$D^c(\alpha) = D(\alpha) + G_0^c \quad \text{with} \quad G_0^c = \omega^c \sum_{n=1}^{N+1} q_n^c C_n(\alpha), \tag{31}$$

where $\omega^c = \pi f_c/f_s$, $\omega_n^c = \omega^c[A]_{n,n}$ (with A given in (19)) and C, D are given by (21-22) for the coefficients $\boldsymbol{\mu}$ computed in section V-B.

D. Stability for time-varying parameters

Equations (27-28) provide a stable system for all parameters $f_c \in [F^-, F^+]$ and $\alpha \in [0,1]$, even when they are time-varying. Indeed, each first order recursive equation provides a stable time-varying system with input U and output Z_n with finite maximal gain G_n: $|a_n^c| < a_n^{max} < 1$ where $a_n^{max} = (\nu + 2\pi F^- \alpha_n)/(\nu - 2\pi F^- \alpha_n)$ so that $|Z_n(m)| \le a_n^{max}|Z_n(m-1)| + U_{max} \le G_n U_{max}$ with $G_n = \frac{1}{1-a_n^{max}}$ and $U_{max} = \sup_{m' \le m} |U(m')|$.

Moreover, coefficients $G^c(\alpha)$ and $D^c(\alpha)$ in the observation equation (28) are all finite and bounded, proving that the result also stands for the output Y.

Note that as coefficients in (28) do not depend on α, this implementation of the filter does not include any memory due to the time-variation of α: this equation renders the output of the filter of order $\alpha(t_m)$ at time t_m as if α had been constant from the initial time.

An illustration is provided in figure 10. In this example, the input is a gaussian white noise. The cutoff frequency and the order are time-vayring with both slow and fast variations. They cover the full range in a non synchronuous way. In spite of these furthest conditions, the stability of the filter appears to be unaltered.

VII. SIMULATION AND RESULTS

The Bode diagrams built from the discrete Fourier transform of simulated outputs are displayed in figures 11-12 for the following choice: the input is a unit pulse so that the output is the impulse response, parameters are constant ($f_c = 200\,\mathrm{Hz}$, $\alpha = \alpha_j$ for $0 \le j \le J = 10$), the weights μ are those obtained in section V-B, the sampling frequency is $F_s = 96\,\mathrm{kHz}$ and the time of simulation is chosen sufficiently long ($T_{simu} = 2^{17}\,F_s^{-1} \approx 1.37\,\mathrm{s}$).

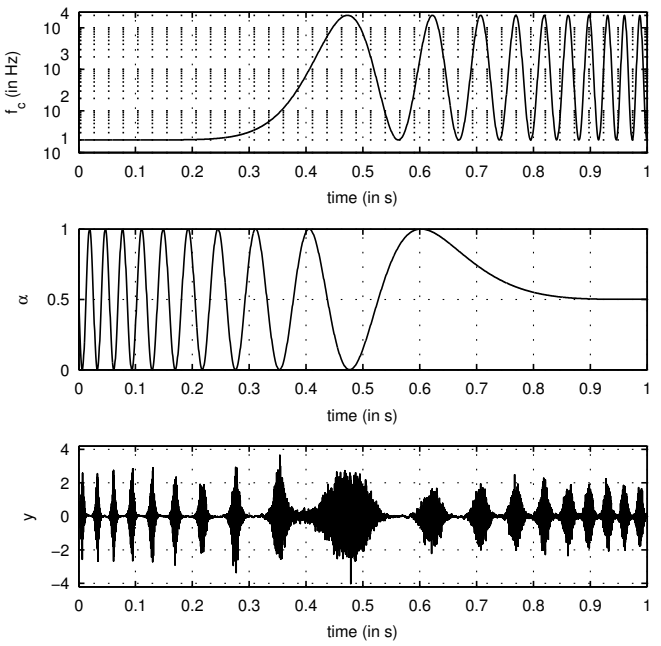

Fig. 10. (Time domain) Simulation with Tustin's method at $f_s = 96\,\mathrm{kHz}$ of the filter fed by a Gaussian white noise with a unitary standard deviation on $0 \le t \le 1s$. Time-varying parameters are such that $\ln f_c(t) = \ln f_c^{min} + (\ln f_c^{max} - \ln f_c^{min})\big(1 - \cos(2\pi\,10\,t^4)\big)/2$ (top) and $\alpha(t) = \alpha^{min} + (\alpha^{max} - \alpha^{min})\,(1 + sin\big(2\pi\,10\,(1-x)^4\big))/2$ (middle) for the maximal parameter ranges ($f_c^{min} = 20\,\mathrm{Hz}$, $f_c^{max} = 20\,\mathrm{kHz}$, $\alpha^{min} = 0$ and $\alpha^{max} = 1$). The output signal y is bounded (bottom).

This discrete Fourier transform is denoted $\breve{F}_{\alpha,f_c}$ so that it cannot be confused with the previous notations (recall that F_{α,f_c}, $\widehat{F}_{\alpha,f_c}$, $\widetilde{F}_{\alpha,f_c}$, respectively denote (i) the exact transfer function, (ii) the finite dimensional approximation in the Laplace(/Fourier) domain and (iii) the finite dimensional approximation in the z-domain according to the numerical scheme).

Results appear to be accurate and the main deviation is observed at 20kHz on the modulus. This is confirmed by computing the errors. Three types of errors (maximal with respect to the cutoff frequency $f_c \in \{20Hz, 200Hz, 2000Hz, 20000Hz\}$ and the fractional order α increasing from 0 to 1 with step 0.1) are characterized in figure 13. They are chosen as follows: the relative error $\big|1 - \breve{F}_{\alpha,f_c}/F_{\alpha,f_c}\big|$, the magnitude deviation in decibels $20\log_{10}|\breve{F}_{\alpha,f_c}| - 20\log_{10}|F_{\alpha,f_c}|$, and the phase deviation $\arg\big(\breve{F}_{\alpha,f_c}/F_{\alpha,f_c}\big)$.

For all the parameter values, the maximal deviations are about 5 on the phase and about about 1.4 dB on the modulus, in the very high frequency range. These deviations are mainly due to the numerical scheme (here, based on the bilinear transform) and could be reduced by increasing the oversampling ratio.

A real-time version of this family of filters has been implemented in FAUST langage [26], which is available for time-varying parameters.

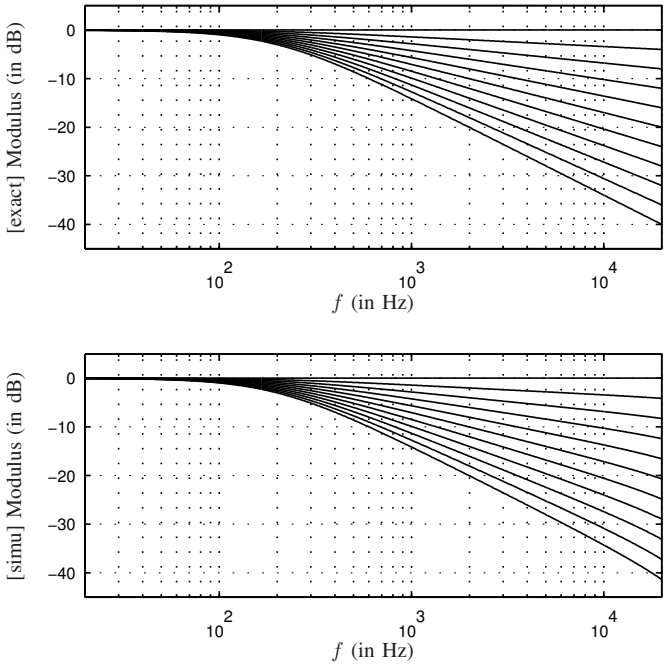

Fig. 11. Magnitude of the Bode diagrams obtained from: (top) the exact transfer function (F_{α,f_c}); (bottom) the discrete Fourier transform of the simulations ($\breve{F}_{\alpha,f_c}$) for the same parameters as in figure 7 and with $f_c = 200\,\text{Hz}$, $F_s = 96\,\text{kHz}$ and $T_{simu} = 2^{17}\,F_s^{-1} \approx 1.37\,\text{s}$.

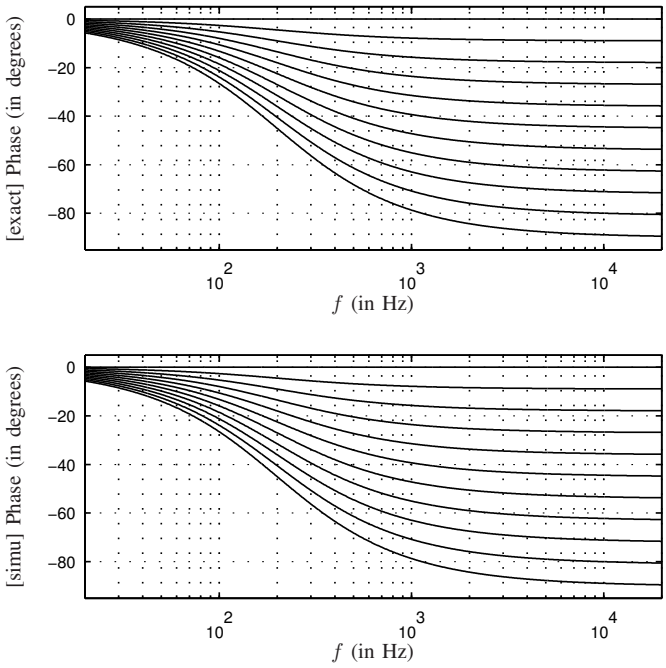

Fig. 12. Phase of Bode diagrams in figure 11.

VIII. Discussion

Although the fractional order filters under consideration are not fractional differential systems, these objects share common properties. One of them is that they both corresponds to pseudo-differential time operators, the spectrum of which is a continuous set (interpreted here as a branch cut which lies on

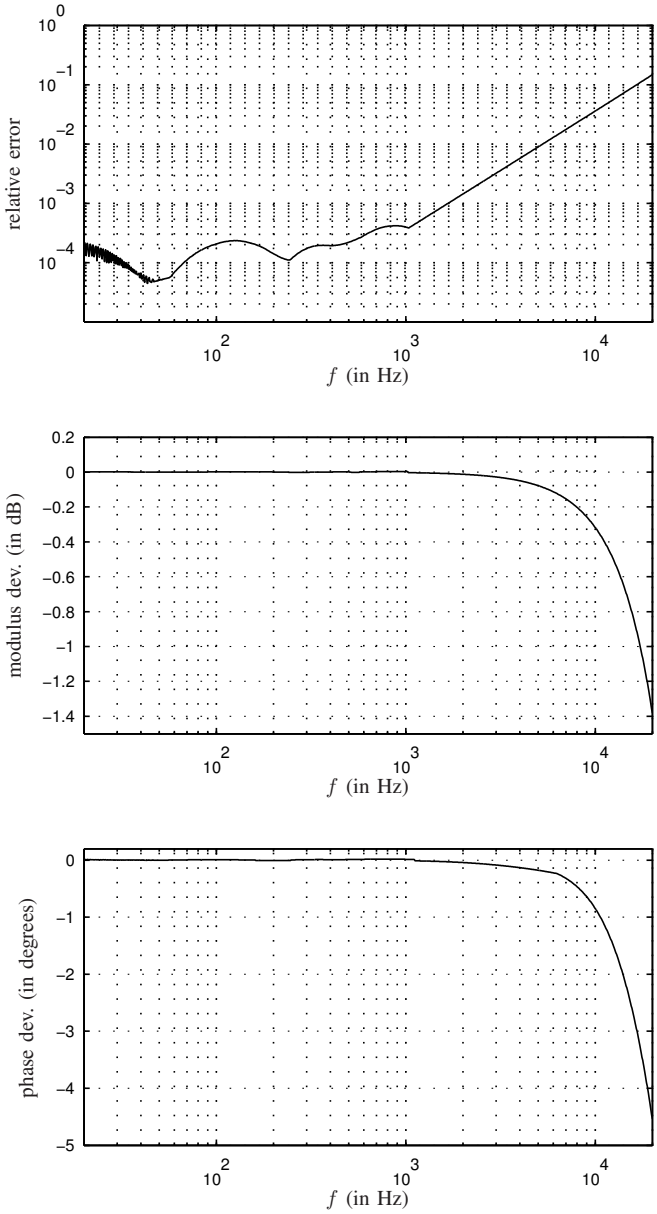

Fig. 13. The "Worst errors" (maximal deviations over $f_c \in \{20Hz, 200Hz, 2000Hz, 20000Hz\}$ and α increasing from 0 to 1 with step 0.1) between the transfer function $\breve{F}_{\alpha,f_c}$ computed from the discrete Fourier transform of simulations and the exact transfer function F_{α,f_c}. Top: relative error $\left|1 - \breve{F}_{\alpha,f_c}/F_{\alpha,f_c}\right|$. Center: magnitude deviation in decibels $20\log_{10}|\breve{F}_{\alpha,f_c}| - 20\log_{10}|F_{\alpha,f_c}|$. Bottom: phase deviation $\arg\left(\breve{F}_{\alpha,f_c}/F_{\alpha,f_c}\right)$ in degrees.

$\mathbb{R}^-$ in the complex Laplace plane). To handle the difficulty due to the infinite dimension of such systems, specific approaches such as that of Grunwald-Letnikov have been developed for fractional integrators and differentiators [7]. Following this approach, a fractional system can be directly converted into a (very large) finite impulse response, which, in a second step, can efficiently be converted into a short infinite impulse response filter by solving a least square problem (see e.g. [27]). Like in this last approach, the method 2 is based on a least square problem. But the particularity is to process the optimization in the Fourier domain in order to avoid some

difficulties and benefit from several advantages, specifically due to the target audio application, namely:

1) the singularity of h_α at $t=0$ would make the problem ill-conditioned in the time domain whereas the criterion $\int_{\mathcal{C}} \left|\frac{\mathrm{d}M_\alpha(\sigma)}{1-\sigma}\right| < +\infty$ is fulfilled, meaning that the integral representation is well-posed and can be used in practice;
2) for audio purposes, the design of the objective function according to perception principles is easier and more efficient in the frequency domain than in the time domain;
3) because of the Parseval theorem, least square problems are well-posed (and equivalent in frequency or the time domain) for systems whose impulse response belongs to $L^2(\mathbb{R}^+)$ (see appendix IX-A). However, as specified in section III-A, for h_α, this is true only if $\alpha > 1/2$. For $\alpha < 1/2$, the energy is no more defined. In the frequency domain, the truncated audio frequency range allows the rejection of this problem, while keeping some sense with respect to the audio objective. The efficiency of the method proposed here and the difficulty for handling this problem are both corroborated by the figure 9 (right): this figure shows that the highest approximation error corresponds orders α lying between $\alpha=0$ and $\alpha=0.5$ but that it is also well-controlled by the optimization.

However, one current limitation of the method 2 is conerned with the choice of the poles: they are not estimated. The heuristic law relying on a quasi-geometric series proves to be relevant: it is naturally adapted to the (audio) log-frequency scale. But, it is certainly not optimal. This is corroborated by the biases that are generated by the interpolation method based on this placement. Some interesting issues could be: (i) locally optimize the poles placements with standard practical methods; (ii) investigate on the convergence of the interpolation method to derive some laws from the weights μ_α; (iii) develop links with the approaches above-mentioned.

IX. Conclusion

In this paper, a new family of low-pass filters has been proposed. It allows the tuning of the cutoff frequency between 20 Hz and 20 kHz and that of the filter attenuation between 0 and -6 decibels per octave, separately and independently from one another. The realization of this family required to optimize finite dimensional approximations of an exact "diffusive representation" of the filters.

In practice, a simulation has been obtained using 13 one-poles filters, the poles of which exclusively depend on the desired cutoff frequency, and using a linear combination of their 13 outputs, the coefficients of which exclusively depend on the desired filter attenuation. This structure guarantees the stability even for time-varying parameters. In this case and with this choice, the simulation renders the memory effect due to the time variation of the cutoff frequency whereas, for the attenuation, it locally renders the output as if the attenuation had been the current value from the initial time. The results are accurate on the complete frequency range.

Perspectives for further work are to consider higher fractional orders and other families of fractional order filters such as high pass filters or resonant filters.

Appendices

A. Recalls on the Hardy spaces and the Paley-Wiener theorem

Let $L^2(\mathbb{R}^+) = \left\{h : \mathbb{R}^+ \to \mathbb{C} \,\middle|\, h \text{ is measurable and } \int_{\mathbb{R}^+} |h(t)|^2 \mathrm{d}t < \infty\right\}$ denote the space of causal functions with finite energy, and

$$\mathbb{H}^m(\mathbb{C}_0^+) = \left\{H : \mathbb{C}_0^+ \to \mathbb{C} \,\middle|\, H \text{ is holomorphic and } \|H\|_{\mathbb{H}^m} = \sup_{\zeta>0}\left[\frac{1}{2\pi}\int_{\mathbb{R}} |H(x+iy)|^m \mathrm{d}y\right]^{\frac{1}{m}} < \infty\right\} \quad (32)$$

denote the Hardy spaces for $m > 0$. The Hardy spaces define transfer functions H of causal systems, that is, the associated convolution kernels h are zero for $t < 0$ (see e.g. [28]). The Paley-Wiener theorem gives the particular following result: under the Laplace transform, $L^2(\mathbb{R}^+)$ is isomorphic to $\mathbb{H}^2(\mathbb{C}_0^+)$ (see e.g. [29, p. 645] or [30]).

The limit Hardy space $\mathbb{H}^\infty(\mathbb{C}_0)$ is the vector space of bounded holomorphic functions that have a finite norm $\|H\|_{\mathbb{H}^\infty} = \sup_{s\in\mathbb{C}_0^+} |H(s)|$. Moreover, for $0 < p \le q \le +\infty$, $\mathbb{H}^q$ is a subset of $\mathbb{H}^p$, and the $\mathbb{H}^p$-norm is increasing with p.

B. Integral representation and Bromwich contour

Consider the (oriented) Bromwich contour $\mathcal{C}_B = \mathcal{C}_1 \cup \mathcal{C}_2^+ \cup \mathcal{C}_3 \cup \mathcal{C}_2^-$ parametrized by $R > \epsilon_x > \epsilon_y > 0$, as described in figure 14.

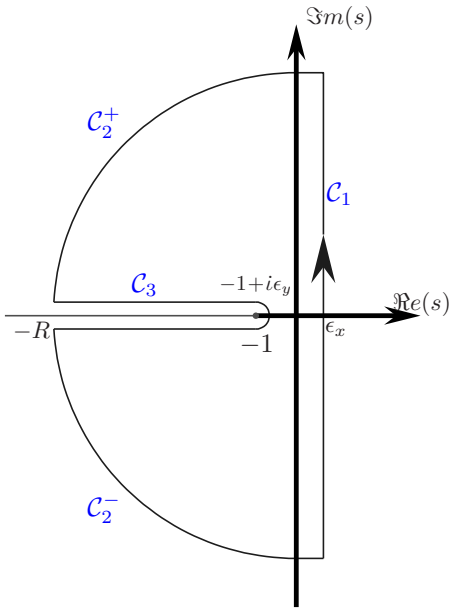

Fig. 14. Bromwich contour adapted to H_α.

Then, denote $I = I_1 + I_2^+ + I_3 + I_2^-$ the integral of $G : s \mapsto \frac{1}{2i\pi} H_\alpha(s)\exp(st)$ onto $\mathcal{C}_B$ with $t > 0$, and define the jump of H_α when s crosses the cut at $\sigma \in \mathcal{C}$, namely,

$$\eta_\alpha(\sigma) = H_\alpha(\sigma - i0^+) - H_\alpha(\sigma + i0^+).$$

From the residue theorem, this integral is $I = 0$, since G is analytic inside $\mathcal{C}_B$. Moreover, as $R \to +\infty$ and $0 < \epsilon_y < \epsilon_x \to 0^+$, each integral absolutely converges

towards the limit $I_1 \to h_\alpha(t)$, $I_2^{\pm} \to 0$ (Jordan's lemma) and $I_3 \to \frac{1}{2i\pi}\int_{\mathcal{C}}[-\eta_\alpha(\sigma)]\,\mathrm{e}^{\sigma t}\,\mathrm{d}\sigma$ so that for all positive t,

$$h_\alpha(t) = \int_{\mathcal{C}} \exp(\sigma t)\ \mu_\alpha(\sigma)\,\mathrm{d}\sigma$$

where $\mu_\alpha(\sigma) = \frac{H_\alpha(\sigma - i0^+) - H_\alpha(\sigma + i0^+)}{2i\pi}$. This is the result given in (6).

REFERENCES

[1] Thomas Hélie. Real-time simulation of a family of fractional-order low-pass filters. In *the 135th Convention of the Audio Engineering Society*, New York, United States, 2013.

[2] D. B. Keele. The design and use of a simple pseudo random pink-noise generator. *Journal of the Audio Engineering Society*, 21(1):33–41, 1973.

[3] M. Abramowitz and I. A. Stegun. *Handbook of mathematical functions*. Dover, New York, 1970.

[4] A. Rumeau. *Modlisation comportementale en gnie lectrique sous reprsentation diffusive: mthodes et applications*. PhD thesis.

[5] Propylene Glycol Dielectric relaxation in Glycole and n Propanol. D.w. davidson and r.h. cole. *Journal of Chemical Physics*, 19:p. 1484–1490, 1951.

[6] R. R. Nigmatullin and Ya. E. Ryabov. Cole-davidson dielectric relaxation as a self-similar relaxation process. *Physics of the Solid State*, 1997.

[7] K. B. Oldham and J. Spanier. *The fractional calculus: theory and application of differentiation and integration of arbitrary order*. Academic press, 1974.

[8] D. Matignon and G. Montseny, editors. *Fractional Differential Systems: models, Methods and Applications*, volume 5. ESAIM Proceedings, SMAI, 1998.

[9] M. D. Ortigueira and F. Coito. From differences to derivatives. *Fractional Calculus and Applied Analysis*, 7(4):459–471, 2004.

[10] A. Oustaloup. *Diversity Fractional Differentiation for System Dynamics*. Wiley-ISTE, 2014.

[11] Denis Matignon. Stability results for fractional differential equations with applications to control processing. In *In Computational Engineering in Systems Applications*, pages 963–968, 1996.

[12] Thomas Hélie and Denis Matignon. Representation with poles and cuts for the time-domain simulation of fractional systems and irrational transfer functions. *Journal of Signal Processing, special issue on Fractional Calculus Applications in Signals and Systems*, 86:2516–2528, 2006.

[13] O. J. Staffans. Well-posedness and stabilizability of a viscoelastic equation in energy space. *Trans. Amer. Math. Soc.*, 345(2):527–575, 1994.

[14] D. Matignon and H. Zwart. Standard diffusive systems as well-posed linear systems. *International Journal of Control*, (accepted), 2013. Paper available at `http://oatao.univ-toulouse.fr/3900/`.

[15] Eberhard Zwicker and Hugo Fastl. *Psychoacoustics: Facts and Models (Springer Series in Information Sciences) (v. 22)*. Springer, 2nd ed. edition, 1999.

[16] D. Heleschewitz. *Analyse et simulation de systmes diffrentiels fractionnaires et pseudo-diffrentiels linéaires sous représentation diffusive*. Thse de doctorat, ENST, 2000.

[17] A. N. Tikhonov, A. V. Goncharsky, V. V. Stepanov, and A. G. Yagola. *Numerical Methods for the Solution of Ill-Posed Problems*. Kluwer Academic Publishers, 1995.

[18] Lennart Ljung. *System Identification: Theory for the User*. Prentice Hall, 2nd ed. edition, 1998.

[19] V.A. Morozov. *Regularization Methods for Ill-Posed Problems*. CRC Press, 1993.

[20] A. Neumaier. Solving ill-conditioned and singular linear systems: A tutorial on regularization. *SIAM*, 40(3):636–666, 1998.

[21] L. F. Shampine. *Numerical Solution of Ordinary Differential Equations*. Chapman & Hall, New York, 1994.

[22] Raymond A. DeCarlo. *Linear Systems: A State Variable Approach with Numerical Implementation*. Prentice Hall, 1989.

[23] M. A. Al-Alaoui. Novel digital integrator and differentiator. *Electron. Lett.*, 29:376–378, 1993.

[24] B. T. Krishna and K. V. V. S. Reddy. Design of digital differentiators and integrators of order 1/2. *World Journal of Modelling and Simulation*, 4(3):182–187, 2008.

[25] V. Havu and J. Malinen. *Numerical Functional Analysis and Optimization*, 28(7-8):825–851, 2007.

[26] *New Computanionals Paradigms for Computer Music*, chapter Faust: an Efficient Functional Approach to DSP Programming. Edition Delatou, 2009. ISBN 978-2-7521-0054-2.

[27] Barbosa, J. Tenreiro Machado, and I. Ferreira. Pole-zero approximations of digital fractional order integrators and differentiators using signal modeling techniques. In *Proceedings of IFAC World Congress*, volume 16, Prague, Czech Republic, 2005. IFAC.

[28] J. J. Benedetto and H. P. Heinig. Weighted hardy spaces and the laplace transform, harmonic analysis. *Lecture Notes in Math., Springer, Berlin*, 992:240–277, 1983.

[29] R.F. Curtain and H.J. Zwart. *An introduction to Infinite-Dimensional Linear Systems Theory*. Springer-Verlag, New York, 1995.

[30] J. R. Partington. *Linear operators and linear systems*. London Mathematical Society Student Texts (No. 60). Cambridge University Press, London, 2004.

Thomas Hélie received the Dipl. Ing. degree from the Ecole Nationale Supérieure des Télécommunications de Bretagne, France, in 1997, the M.S. degree in acoustics, signal processing, and informatics applied to music, Université Paris 6, France, in 1999, the M.S. degree in automatic and signal processing from the University Paris-Sud, in 1999, and the Ph.D. degree in automatic and signal processing from University Paris-Sud in 2002. After postdoctoral research in the Laboratory of Nonlinear System at the Swiss Federal Institute of Lausanne, Lausanne, Switzerland, in 2003 and a Lecturer position at the University Paris-Sud in 2004, he has been, since 2004, Researcher at the National Research Council, Analysis/Synthesis Team, IRCAM-CNRS UMR 9912 - UPMC, Paris. His research topics include audio processing, physics of musical instruments, physical modeling, nonlinear dynamical systems, and inversion processes.